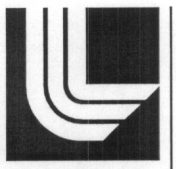

LAWRENCE
LIVERMORE
NATIONAL
LABORATORY

UCRL-JC-155503

Electrochemical Testing of Gas Tungsten Arc Welded and Reduced Pressure Electron Beam Welded Alloy 22

S.D. Day, F.M.G. Wong, S.R. Gordon, L.L. Wong, R.B. Rebak

September 7, 2003

Effect of Processing on Materials Properties for Nuclear Waste Disposition, Symposium of the 2003 MS&T Conference, Joint Meeting between 2003 Fall Meeting of TMS and the 45th ISS, Chicago, IL, November 9 – 12, 2003

This work was performed under the auspices of the U.S. Department of Energy by University of California, Lawrence Livermore National Laboratory under Contract W-7405-Eng-48.

07 September 2003
Paper to be published in the proceedings of the "Effect of Processing on Materials Properties for Nuclear Waste Disposition" Symposium of the 2003 MS&T '03. Conference, which is a joint meeting between the 2003 Fall Meeting of TMS (The Minerals, Metals and Materials Society) and the 45th ISS (Iron and Steel Society), 9-12 November 2003 – Chicago, IL

Electrochemical Testing of Gas Tungsten Arc Welded and Reduced Pressure Electron Beam Welded Alloy 22

S. Daniel Day, Frank M. G. Wong, Steven R. Gordon, Lana L. Wong and Raúl B. Rebak
Lawrence Livermore National Laboratory
7000 East Ave, Livermore, CA 94550

ABSTRACT

Alloy 22 (N06022) is the material selected for the fabrication of the outer shell of the nuclear waste containers for the Yucca Mountain high-level nuclear waste repository site. A key technical issue in the Yucca Mountain waste package program has been the integrity of container weld joints. The currently selected welding process for fabricating and sealing the containers is the traditional gas tungsten arc welding (GTAW) or TIG method. An appealing faster alternative technique is reduced pressure electron beam (RPEB) welding. Standard electrochemical tests were carried on GTAW and RPEB welds as well as on base metal to determine their relative corrosion behavior in SCW at 90°C (alkaline), 1 M HCl at 60°C (acidic) and 1 M NaCl at 90°C (neutral) solutions. Results show that for all practical purposes, the three tested materials had the electrochemical behavior in the three tested solutions.

Keywords: N06022, Gas Tungsten Arc Welding, Reduced Pressure Electron Beam Welding, General Corrosion, Localized Corrosion

INTRODUCTION

Alloy 22 (N06022) is the material selected for the fabrication of the outer shell of the nuclear waste containers for the Yucca Mountain nuclear waste repository site [1,2]. Its selection has been based on its overall resistance to corrosion in both oxidizing and reducing environments, and its successful use in extremely aggressive industrial applications. Alloy 22 has been shown to have a much greater resistance than conventional stainless steel grades to pitting corrosion and stress corrosion cracking in chloride-bearing environments [3-7]. Extensive welding will be used to fabricate the containers. For example, for the outer lid it is expected to have three circumferential and one longitudinal weld seams. Roughly, each container will have more than 20 m of weld seam that would be exposed to the environment at the permanent emplacement site in Yucca Mountain. In industrial applications it is generally regarded that weld seams are the most vulnerable components in the equipment since welds can be sites of residual stress that could promote stress corrosion cracking and metallurgical heterogeneity that could promote localized corrosion under favorable electrochemical and environmental conditions. The current candidate welding process to fabricate the waste container is the classic gas tungsten arc welding (GTAW) or TIG technique. Another appealing procedure is the reduced pressure electron beam (RPEB) method, recently developed in the United Kingdom. The RPEB welding method is particularly appealing for the welding of thick plates since it requires only one pass as compared to multiple passes for the GTAW. Another benefits is that RPEB does not require filler metal; that is, it is autogenous and also does not require extensive plate machining prior to welding.

Figure 1 shows a macrograph of the cross section of a 1.5-inch thick Alloy 22 plate that was welded using the GTAW technique. This was a double V welding that consisted of at least nine passes on each side of the plate. Figure 1 shows that the width of the weld seam was up to 20 mm in the outside surface and approximately 10 mm wide in the middle section of each V (at one fourth of the plate thickness). Figure 2 shows a macrograph of the cross section of a 1.5-inch thick plate that was welded using the RPEB technique. This was a single pass autogenous weld, with a maximum width at the surface of 10 mm and a rather constant weld seam width through the thickness of the plate of 3 mm. Comparing Figures 1 and 2, it is obvious that the RPEB plate contains less amount of weld material than the GTAW plate.

The current study was undertaken to examine the relative corrosion resistance of Alloy 22 in three conditions: (1) base metal, (2) GTAW and (3) RPEB. The general and localized corrosion studies of the three types of material were carried out in three different electrolyte solutions. These were Simulated Concentrated Water (SCW), One Molar Hydrochloric Acid (1 M HCl) and One Molar Sodium Chloride (1 M NaCl) solutions. SCW was used as a representative environment of Yucca Mountain since SCW is approximately 1000 times more concentrated than the well J-13 water from near Yucca Mountain. SCW is slightly alkaline (pH between 8 and 10). The 1 M HCl at 60°C environment was used since it can etch welds under positive polarization. The pH of 1 M HCl is zero (highly acidic). The saline solution 1 M NaCl at 90°C was used since it is one of the least aggressive

environments that can still promote crevice corrosion in Alloy 22 at anodic applied potentials. The pH of 1 M NaCl is near neutral.

EXPERIMENTAL PROCEDURES

The test pieces were water jet-cut from a 1.25-inch thick Alloy 22 plate containing GTAW and RPEB weld seams. Framatome (USA) performed the GTAW welding and the TWI (UK) carried out the RPEB welding. The heat of the base metal was 059902LL1 and the heat of the weld wire used for the GTAW was XX1753BG. The compositions of these heats are given in Table 1. The different specimens were manufactured by CTC-United Defense in Santa Clara, CA and surface finished at Lawrence Livermore National Laboratory (LLNL). These were of 0.625-inch diameter disks (ASTM G 5) [8] and standard MCA (multiple crevice assembly) specimens. The disks were prepared from five cores taken through the weld plate from the beam or arc side to the opposite surface. Four disks were sliced from each core, one from the top surface (A) and one from the bottom surface (D), and two from locations one-third (B) and two-thirds (C) the distance between these surfaces. The specimens used in this study were from the top surface (A) and the one-third depth level (B) beneath it. The GTAW weld specimen series is designated GXXX and the RPEM weld series 15XXX. Separate Alloy 22 base metal disks in the mill-annealed (MA) condition that were not taken from this weld plate are labeled DEAXXXX. The MCA specimens lie in the plate plane with the weld seams cutting across the loop end, perpendicular to the stem direction. The MCA specimens were taken from the same sampling levels (A through D) as the disks.

Most of the test specimens were disk assemblies designed to test for general corrosion and passivity according to ASTM G 5 guidelines. The MCA specimens were assembled using a Teflon-coated ceramic washer for crevice forming as described in ASTM G 48 [8]. The tested surface area of the disk specimens was approximately 0.7 cm^2 and the exposed MCA specimen area was about 5.6 cm^2. The test specimens were given a 600 grit silicon carbide abrasive paper finish approximately one hour prior to testing. They were then ultrasonicated in distilled water for 5 minutes and then degreased with acetone, isopropyl alcohol, and distilled water.

Electrochemical tests were carried out in deaerated solutions of SCW (1000 times the concentration of Yucca Mountain J-13 well water; see Table 2 for chemistry), 1 M HCl, and 1 M NaCl. The SCW has a pH of about 10.2 The pH of the NaCl solution was approximately 7 and the hydrochloric acid solution had a pH of 0. The SCW and 1 M NaCl test temperature was 90°C and the 1 M HCl tests were carried out at 60°C. Nitrogen (N_2) was bubbled through the solution at a flow rate of 100cc/min for the duration of the electrochemical tests. The corrosion potential (E_{corr}) was monitored for 1 hour, and was immediately followed by three consecutive polarization resistance (PR) tests (ASTM G 59) [8] and one cyclic polarization (CP) test (ASTM G 61) [8]. The electrochemical tests were carried out in a one-liter, three-electrode, borosilicate glass flask (ASTM G 5). Figures 3 and 4 show the Alloy 22 test specimen assemblage for the discs and MCA, respectively. A water-cooled condenser combined with a water trap was used to maintain solution concentration

and a controlled atmosphere. Solution temperatures were maintained by partially immersing the cell in a thermostat-controlled silicone oil bath. All the tests were conducted at ambient pressure. The reference electrode was a saturated silver chloride (SSC) electrode, which has a potential 199 mV more positive than the standard hydrogen electrode (SHE). The reference electrode was connected to the solution through a water-cooled Luggin probe to keep it near ambient temperature. The counter electrode was a flag (36 cm^2) of platinum foil spot-welded to a platinum wire. All the potentials in this paper are reported in the SSC scale.

The corrosion rates (CR) were obtained using the polarization resistance method (ASTM G 59). An initial applied voltage 20 mV below the corrosion potential (E_{corr}) was ramped up to a final potential of 20 mV above E_{corr} at a rate of 0.167 mV/s. Linear fits were constrained to a potential range of 10 mV below E_{corr} to 10 mV above E_{corr}. The Tafel constants, β_a and β_c, were assumed to be $\pm$ 0.12 V/decade. Corrosion rates were calculated using Equation 1:

$$CR(nm/yr) = k\frac{i_{corr}}{\rho}EW \qquad (1)$$

where k is a conversion factor (3.27 x 10^9 $nm \cdot g \cdot A^{-1} \cdot cm^{-1} \cdot yr^{-1}$), i_{corr} is the measured corrosion current density in A/cm^2, EW is the equivalent weight (23.28 g/mol), and ρ is the density of Alloy 22 (8.69 g/cm^3).

Tests to assess the susceptibility of the Alloy 22 welds to localized corrosion and passive stability were conducted using the cyclic potentiodynamic polarization technique (ASTM G 61). The potential scans began 50 mV below E_{corr} using a set scan rate of 0.167 mV/s. The scan direction was usually reversed when the current density reached 5 mA/cm^2 in the forward scan. After the cyclic polarization tests the specimens were examined in an optical stereomicroscope at a 40X magnification to establish the mode of attack. Selected specimens were also imaged using a scanning electron microscope (SEM).

One specimen of each weld type (GTAW and RPEB) was subjected to galvanostatic (constant current density) testing in the HCl solution to reveal weld areas that were more susceptible to corrosion. The galvanostatic tests were preceded by a 1 hour open circuit potential run and three linear polarizations scans to measure corrosion rates. The galvanostatic procedure passes current through the specimen to maintain a fixed current density for a given length of time. The initial test pair (G04A and 1504A) was exposed to a current density of 0.1 mA/cm^2 for 3 hours. The resulting corrosion features were mild enough to require a second test at a higher current density of 1 mA/cm^2 using specimens G03A and 1503A. The latter specimens showed significant corrosion features to merit SEM imaging and EDS analysis. The images and major element compositional data will be used to document the susceptibility of different regions or phase domains in the welds to generalized corrosion.

RESULTS AND DISCUSSION

The Corrosion Potential (E_{corr})

Figures 5-7 and show the evolution the corrosion potentials (E_{corr}) of Alloy 22 for 1 hour for GTAW, RPEB and base metal specimens in SCW, 1 M HCl, and 1 M NaCl solutions. A one-hour interval may not be sufficient for the corrosion potential to reach a steady state value. A complete comparison of the E_{corr} evolution between solution and solution is not possible since 1 M HCl was at 60°C and the other two (NaCl and SCW) were at 90°C. In general, Figures 5-7 show that E_{corr} initially increased in the SCW and 1 M NaCl solutions, and decreased in the 1 M HCl solution. The amount of change was more pronounced in the SCW and 1 M NaCl solution. These two latter solutions are not as corrosive as the 1 M HCl solution and therefore, E_{corr} increased as a protective oxide film was forming on the surface of the specimens. Figure 7 shows that the E_{corr} values are highly reproducible between run and run, especially for the 1 M HCl solution.

Figure 8 shows the evolution of E_{corr} for GTAW and RPEB welded material discs in SCW and 1 M HCl solution. Also, Figure 8 shows the E_{corr} for each type of weld at the two different levels. Level A corresponded to the outermost layer of the plate and level B was the following level. Since the SCW solution is not as corrosive, there was not a clear trend on the values of E_{corr} based on the type of weld. Similarly, there was not a specific trend on the E_{corr} based on the level (A or B) the specimen was removed from in each weld condition (GTAW and RPEB). Figure 8 also shows that in the HCl solution, it appears that the level A specimens (both for GTAW and RPEB) were slightly more active than the level B specimens. However, there is not a clear trend between types of weld.

Table 3 and Figure 9 show the E_{corr} values after a 1 h immersion for discs (in HCl and SCW) and MCA specimens (in NaCl). The E_{corr} for the base MCA are for 24 h immersion. It is clear that the E_{corr} for Alloy 22 in HCl solution are highly reproducible and non dependent on the type of material (GTAW, RPEB or Base). For the SCW and NaCl solutions, the values of E_{corr} were more scattered (because the solutions are less aggressive); however, it appears that the welds were more noble (higher E_{corr}) than the base material.

Corrosion Rates from Polarization Resistance (PR) Tests

Table 3 shows corrosion rates as a function of the type of material in SCW at 90°C, 1 M HCl at 60°C and 1 M NaCl at 90°C solutions. Figure 10 shows the corrosion rates for the three types of material (GTAW, RPEB and Base discs) in SCW at 90°C (Table 3). Figure 10 shows that the lowest corrosion rate corresponded to the base metal with an average value of 0.8 μm/year. The second lowest corrosion rate corresponded to the GTAW material with an average value of 1.3 μm/year and the highest corrosion rate corresponded to the RPEB material with an average corrosion rate of 2 μm/year. Figure 10 shows that the corrosion rate of the GTAW material was consistently lower than the RPEB material. (CR GTAW/CR RPEB = 0.65).

Figure 11 shows the corrosion rates for the three types of material (GTAW, RPEB and Base discs) in 1 M HCl at 60°C (Table 3). In this aggressive environment, the lowest corrosion rate corresponded to GTAW with an average value of 280 μm/year. The second lowest corrosion rate corresponded to the RPEB material with an average value of 335 μm/year and the highest corrosion rate corresponded to the base metal with and average value of 380 μm/year. This behavior was totally unpredictable since it was initially assumed that the welds would corrode faster in this acidic solution. Similar to the behavior of welds in SCW solution (Figure 10), the corrosion rate of the GTAW material was lower than the corrosion rate of the RPEB material (CR GTAW/CR RPEB = 0.84).

Figure 12 shows the corrosion rates for the three types of material (GTAW, RPEB and Base MCA specimens) in 1 M NaCl at 90°C (Table 3). In this saline solution the lowest corrosion rate also corresponded to the GTAW material with an average value of 0.6 μm/year. The second lowest corrosion rate was for the RPEB material with an average value of 0.8 μm/year and the highest corrosion rate was for the base material with an average value of 1.9 μm/year. Similar to the behavior of welds in SCW and HCl solutions (Figures 10 and 11), the corrosion rate of the GTAW material was lower than the corrosion rate of the RPEB material (CR GTAW/CR RPEB = 0.75).

Figure 13 shows the relative corrosion rates for the three materials (GTAW, RPEB and Base) in the three tested solutions. Figure 13 clearly shows that the corrosion rate in the 1 M HCl solution was approximately two orders of magnitude higher than in the other two less aggressive solutions. The overall lowest corrosion rates were for the 1 M NaCl solution on MCA (creviced) specimens.

Potentiodynamic Cyclic Polarization (PCP)

Figures 14-16 show the cyclic polarization behavior of Alloy 22 GTAW, RPEB, and base metal specimens in deaerated SCW at 90°C, 1 M HCl at 60°C, and 1 M NaCl at 90°C solutions, respectively. For each solution, the cyclic polarization curves appear almost undistinguishable from each other for the three types of material (GTAW, RPEB and base). Figure 14 shows that for the SCW at 90°C solution, the cyclic polarization curves for all the materials show an anodic peak on the forward sweep at a potential of approximately 250 mV (SSC) with a current density between 350 to 550 $\mu A/cm^2$. The highest current density was for the base material and the lowest for the GTAW specimen. The origin of these peaks is still unknown. There is also some noise in the final portion of the reverse scan where it crosses the forward passive region. The origin of this noise is also not known. Even though Figure 14 shows a small hysteresis in the reverse potential scanning, none of the materials tested in SCW at 90°C showed localized corrosion.

Figures 17 and 18 show images of the GTAW and RPEB specimens, respectively, after the cyclic polarization experiments in SCW at 90°C. The GTAW specimen shows fewer amount of cavities on the surface than the RPEB specimen. Moreover, the cavities in the GTAW specimen seemed random while the cavities in the RPEB specimen seemed aligned, probably following freezing patterns in the weld pool.

Figure 15 shows that the cyclic polarization curves for the three materials in 1 M HCl at 60°C almost completely overlap. The largest current density for the anodic peak above the corrosion potential corresponded to the RPEB material (Figure 15). The breakdown potentials (E20 and E200 in Table 3) in 1 M HCl were almost identical for all three materials and well above +0.9 V SSC. None of the materials showed localized corrosion (pitting corrosion) after the potentiodynamic tests despite they were polarized to high anodic potentials in a 1 M chloride solution of pH = 0.

Figure 16 shows the cyclic polarization curves for GTAW and RPEB materials in 1 M NaCl at 90°C. Both curves were similar to each other and exhibited a reverse scan hysteresis loop that intersected the passive current line at –50 to –75 mV SSC. Microscopy of the specimens after the tests showed that both types of materials suffered crevice corrosion under the crevice formers. There was only one test for each welding condition so it is difficult to rank these two materials regarding their relative resistance to localized corrosion. In both types of material the crevice corrosion nucleated and developed both in the welded part of the specimen and also in the base metal. This was clearer to observe in the RPEB material since the weld seam was narrower. Figures 19 and 20 show SEM images of the localized corrosion in the GTAW specimen and Figures 21 and 22 show SEM images of the localized corrosion in the RPEB specimen. Figure 21 shows the band of the weld seam and the outline of one of the crevice formers. It is clear that crevice corrosion nucleated in the boundary between the base metal and the weld seam and in the base metal away from the weld seam. That is, there was not preferential attack by crevice corrosion in the weld seam.

Parameters from the Cyclic Polarization Curves During Localized Corrosion

In polarization curves (e.g. Figures 15 and 16) several specific potential values can be measured. One is the potential at which the net applied cathodic and anodic currents are equal, which is defined as the corrosion potential. Another is the breakdown potential, measured on the forward sweep, where the current density increases significantly and rapidly above the passive current density. Generally, the values of passive current density for Alloy 22 are between 1 $\mu A/cm^2$ and 20 $\mu A/cm^2$. That is, in the forward scan, when the current density reaches 200 $\mu A/cm^2$ the alloy could be considered depassivated. Similarly, when the current density in the reverse scan lies between 10 $\mu A/cm^2$ and 1 $\mu A/cm^2$, the alloy would have regained its passive behavior prior to the breakdown. Hence, parameters can be extracted from the cyclic polarization curves that indicate the potentials at which the forward current density reached 20 $\mu A/cm^2$ (E20) and 200 $\mu A/cm^2$ (E200), and where the reverse current density reached 10 $\mu A/cm^2$ (ER10) and 1 $\mu A/cm^2$ (ER1). These values of characteristic potentials are listed in Table 3. These parameters allow comparison among polarization curves without the clutter of superimposing too many curves. For example, two parameters (E200 and ER10) could capture the basic shape of the potentiodynamic curves. The technique of selecting potential values for fixed current densities has been used before.

The analysis of the parameters from the polarization curves will be done just for the 1 M NaCl solution since this was the only solution that promoted localized corrosion. Figures 23 and 24 show the E_{corr} and the characteristic potentials E200 and ER10 (Table 3) in 1 M NaCl at 90°C. E200 represents the breakdown potential and ER10 represents the

repassivation potential. For example, the difference between E_{corr} and E200 (ΔE=E200-E_{corr}) provides a potential range that the alloy needs to overcome before a faster dissolution rate due to localized corrosion is achieved. Similarly, the difference between E_{corr} and ER10 (ΔE=ER10-E_{corr}) shows the margin of safety that the alloy has in the case that localized corrosion had initiated and needs to be repassivated. That is, if this potential difference ΔE is positive, the alloy could be considered protected against catastrophic corrosion losses by localized attack (or transpassive dissolution in cases where localized corrosion is not found). Figures 23 and 24 show that in both cases (breakdown and repassivation), ΔE is positive and large (> 300 mV) for all tested materials (welded and base). The largest ΔE corresponded to the base metal. Both welded materials (GTAW and RPEB) had similar values of ΔE; however, these values correspond to only one tested specimen of each welded material. These preliminary results indicate that crevice corrosion would not occur in Alloy 22 base and welded at the corrosion potential. A polarization of several hundred mV (Figures 16 and 23) would be needed for localized corrosion to nucleate and propagate.

Galvanostatic Studies

Galvanostatic studies were carried on to etch the weld seam in GTAW and RPEB specimens. Two sets of experiments were carried out in 1 M HCl solution at 60°C. In the first set, a current density of 0.1 mA/cm^2 was applied to the specimens for 3 h. In the second set, a ten times higher current density of 1 mA/cm^2 was applied for the same period. Figure 25 shows the potential output plots for the two applied constant current density tests. Both types of weld show the same applied potential for each applied current density. At the higher applied current density, the output potential was slightly higher (~ 30 mV) for both types of welds (Figure 25). The values of output potential are the same as in the polarization curve (Figure 15).

Figures 26 and 27 show the macro appearance of the corroded RPEB and GTAW specimens after the galvanostatic tests for the 1 mA/cm^2 applied current density. Figures 26 and 27 show that both weld seams were preferentially etched. Figure 26 shows that the weld seam in the RPEB welded specimen was much narrower than the weld seam in the GTAW specimen (Figure 27). This agrees with the macro-etch appearances of the cross section of the weld (Figures 1 and 2).

Figures 28-30 show SEM images of the corroded RPEB welded specimen after the galvanostatic treatment. The corrosion pattern of the weld seam seems to follow specific directions, probably similar to those observed after the cyclic polarization in SCW solution (Figures 14 and 18). That is, by forcing the alloy to corrode at a constant current density, some areas of the weld seam appear to corrode preferentially to other areas (Figure 28). Figure 29 shows the pattern at the center fusion line of the RPEB weld seam; where 45° attacked lines seem to meet (arrows). Figure 30 shows the grain boundary etching appearance of the base metal in the vicinity of the weld seam. This corrosion pattern is typical of N06022 corroding in hot HCl solutions.

Figures 31 and 32 show SEM images of the corroded GTAW welded specimen after the galvanostatic treatment. Figure 31 shows a random appearance of the corrosion pattern of the weld seam in the GTAW as compared to the RPEB weld seam (Figures 28 and 29). Similar to Figure 30, Figure 32 shows grain boundary etching in the base metal part of the GTAW specimen.

Concluding Remarks

Preliminary work to evaluate the anodic behavior of Alloy 22 gas tungsten arc welds and reduced pressure electron beam welds in three test solutions has been completed. The test solutions were chosen to study the weld susceptibility to generalized corrosion, to localized/crevice corrosion, and to compare weld behavior in an anticipated waste container surface solution from the geological repository. No visible evidence of localized corrosion was seen in specimens from the SCW at 90°C and 1 M HCl at 60°C solutions, although passive film breakdown and repassivation were observed in the cyclic polarization scans. The 1 M NaCl at 90°C MCA tests displayed crevice corrosion in both the weld zone and the base metal for each weld type. The GTAW specimens had slightly lower corrosion rates in the test solutions than the RPEB specimens. The GTAW specimens also had slightly more positive breakdown potential ranges above E_{corr} and larger critical potential gaps (ER10 potential minus E_{corr}) than the RPEB specimens. Although these imply superior stability under anodic conditions, the actual values for both welds were quite close in all the three solutions. A factor neglected in this testing was the effect of exposed weld area on specimen electrochemical behavior. This could be significant, since the tungsten arc welds were approximately twice the width of the electron beam welds. Additional work to characterize weld corrosion behavior using SEM-EDS microanalytical techniques could be used to improve the Alloy 22 electron beam welding process and capitalize on its desirable features for cost-effective waste container fabrication.

CONCLUSIONS

(1) The Gas Tungsten Arc Welded (GTAW) weld seam was wider than the Reduced Pressure Electron Beam (RPEB) weld seam

(2) The Corrosion Potential (E_{corr}) in SCW and 1 M NaCl solutions of the GTAW material was slightly more noble than for the RPEB and base materials. In the 1 M HCl solution, E_{corr} of all three materials was undistinguishable from each other.

(3) The corrosion rate of the RPEB welded specimens was of the same order of magnitude than the GTAW and the base materials. However, it is appears that the corrosion rate of the RPEB material was slightly higher than of the GTAW material. This is not relevant for all practical purposes.

(4) All three materials (GTAW, RPEB and Base) showed identical anodic behavior through cyclic polarization in acidic (HCl), neutral (NaCl) and alkaline (SCW) solutions.

(5) Both GTAW and RPEB welded material showed the same susceptibility to localized (crevice) corrosion in 1 M NaCl solutions. Moreover, in each material, the weld seam was not more susceptible to localized corrosion than the adjacent base metal.

(6) The corrosion pattern after the tests seemed slightly more oriented or predisposed in the RPEB material than in the GTAW, which appeared more random.

(7) Overall, the electrochemical properties of the GTAW specimens were slightly superior to those of the RPEB weld specimens regarding passive film breakdown, film repassivation behavior, and corrosion rates. These observations are only result of laboratory testing and may not represent any advantage from an industrial application point of view.

REFERENCES

1. Yucca Mountain Science and Engineering Report, U. S. Department of Energy, Office of Civilian Radioactive Waste Management, DOE/RW-0539, Las Vegas, NV, May 2001.
2. J. H. Lee, K. G. Mon, D. E. Longsine, B. E. Bullard and A. M. Monib in Scientific Basis for Nuclear Waste Management XXV, Vol. 713, pp. 61-70 (Warrendale, PA: Materials Research Society 2002)
3. P. E. Manning, J. D. Schöbel, Werkstoffe und Korrosion, 37, 137-145 (1986).
4. K. A. Gruss, G. A. Cragnolino, D. S. Dunn, N. Sridhar, Paper 149, Corrosion/98 (Houston, TX: NACE International 1998).
5. R. B. Rebak and P. Crook, in Critical Factors in Localized Corrosion III, Vol. 98-17, pp. 289-302 (Pennington, NJ: The Electrochemical Society 1999).

6. R. B. Rebak in Environmentally Assisted Cracking: Predictive Methods for Risk Assessment and Evaluation of Materials, Equipment and Structures, STP 1401, pp. 289-300 (West Conshohocken, PA: ASTM 2000).
7. R. B. Rebak in Corrosion and Environmental Degradation, Volume II, pp. 69-111 (Weinheim, Germany: Wiley-VCH 2000).

Table 1: Chemical Composition of the Studied Alloy 22 Heats (in Wt %)

Element	Base Metal 1.25-inch thick Plate (Heat 059902LL1 by Allegheny Ludlum)	Filler Metal 0.045-inch dia. Wire for GTAW (Heat XX1753BG by Inco Alloys International)
C	0.005	0.004
Co	0.01	0.03
Cr	20.38	20.54
Cu	0.01	0.04
Fe	2.85	2.08
Mn	0.16	0.2
Mo	13.82	14.00
Ni	59.56	59.70
P	0.008	0.004
S	0.0002	0.001
Si	0.05	0.06
V	0.17	0.03
W	2.64	3.10

Table 2: Ionic composition of SCW (simulated concentrated water)

Composition of SCW (Simulated Concentrated Water) in mg/L									
K^+	Na^+	Mg^{2+}	Ca^{2+}	F^-	Cl^-	NO_3^-	SO_4^{2-}	HCO_3^-	SiO_2 (aq)
3400	40,900	<1	<1	1400	6700	6400	16,700	70,000	~40

Table 3: Test conditions and results (with selected potentials from the cyclic polarization curves)

Specimen ID (1)	Type of Material	Electrolyte, Temperature (°C)	1-h E_{corr} (mV, SSC)	Corrosion Rates (μm/year)	E20 (mV, SSC)	E200 (mV, SSC)	ER10 (mV, SSC)	ER1 (mV, SSC)
G01B	GTAW	SCW, 90°C	-418.6	1.232, 1.164, 1.034	170.4(AP), 648.2	668.1	571.9	568.6
G03A	GTAW	SCW, 90°C	-241.6	1.549, 1.351, 1.243	177.0(AP), 654.9	674.8	575.2	568.6
G03A (V)	GTAW	1M HCl, 60°C	-167.4	246.9, 238.8, 269.5	N/A	N/A	N/A	N/A
G03B	GTAW	SCW, 90°C	-242.5	1.431, 1.340, 1.315	180.3(AP), 651.5	674.8	575.2	558.6
G04A (V)	GTAW	1M HCl, 60°C	-171.5	357.1, 360.8, 393.8	N/A	N/A	N/A	N/A
G05A	GTAW	1M HCl, 60°C	-177.7	225.8, 253.7, 271.2	929.2	960.2	902.7	823.0
G05B	GTAW	1M HCl, 60°C	-170.4	228.4, 240.0, 263.2	929.2	955.8	902.7	823.0
G08A	GTAW	1M NaCl, 90°C	-337.2	0.649, 0.605, 0.522	362.8	678.1	17.7	-78.5
1501B	RPEB	SCW, 90°C	-434.8	1.999, 1.614, 1.652	N/A	N/A	N/A	N/A
1503A	RPEB	SCW, 90°C	-288.0	2.609, 2.645, 2.809	183.6(AP), 664.8	688.1	581.9	575.2
1503A (V)	RPEB	1M HCl, 60°C	-172.1	300.7, 308.5, 326.5	N/A	N/A	N/A	N/A
1503B	RPEB	SCW, 90°C	-254.3	1.499, 1.393, 1.373	183.6(AP), 671.5	691.4	588.5	581.9
1504A (V)	RPEB	1M HCl, 60°C	-167.6	316.7, 319.5, 336.0	N/A	N/A	N/A	N/A
1505A	RPEB	1M HCl, 60°C	-177.2	375.1, 395.8, 426.3	933.6	960.2	907.1	823.0
1505B	RPEB	1M HCl, 60°C	-170.0	281.6, 308.6, 318.3	924.8	955.8	902.7	823.0
1508A	RPEB	1M NaCl, 90°C	-353.1	0.754, 0.823, 0.737	269.9(AP), 488.9	691.4	1.1	-58.6
DEA1051	Base	SCW, 90°C	-439.3	0.786, 0.693, 0.611	183.6(AP), 664.8	688.1	588.5	568.6
DEA1052	Base	SCW, 90°C	-415.8	1.096, 0.859, 0.827	183.6(AP), 648.2	664.8	578.5	555.3
DEA1053	Base	1M HCl, 60°C	-176.1	369.2, 413.3, 448.1	924.8	955.8	902.7	827.4
DEA1054	Base	1M HCl, 60°C	-172.5	324.1, 353.8, 388.0	933.6	960.2	907.1	831.9
DEA3143	Base	1M NaCl, 90°C	-405	3.48, 4.45, 2.25	-251(AP), 510	740	64	-70
DEA3144	Base	1M NaCl, 90°C	-446	3.38, 3.84, 11.63	-277(AP), 503	722	46	-92
DEA3262	Base	1M NaCl, 90°C	-571	2.28, 1.59, 1.32	422	709	96	-72
DEA3263	Base	1M NaCl, 90°C	-594	2.77, 2.43, 1.28	386	703	81	-77

(1) For SCW and HCl solutions the specimens were discs and for the NaCl solution they were multiple crevice assemblies (MCA).
(V) The specimen was used for galvanostatic test (Figure 25).
(AP) anodic peak
NA = Not Available or Not Applicable

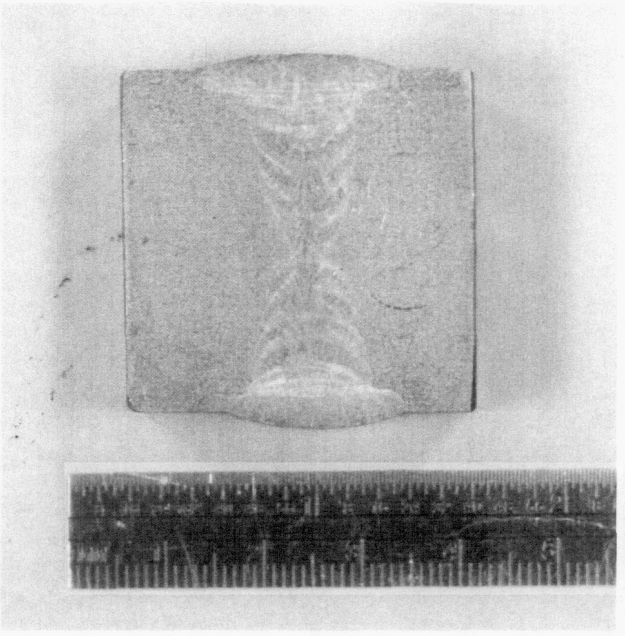

Figure 1: Macrograph of a GTAW welded Alloy 22 plate

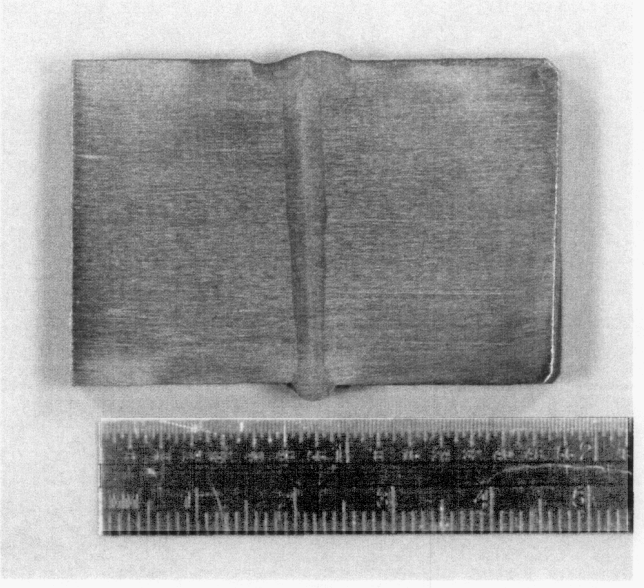

Figure 2: Macrograph of a RPEB welded Alloy 22 plate

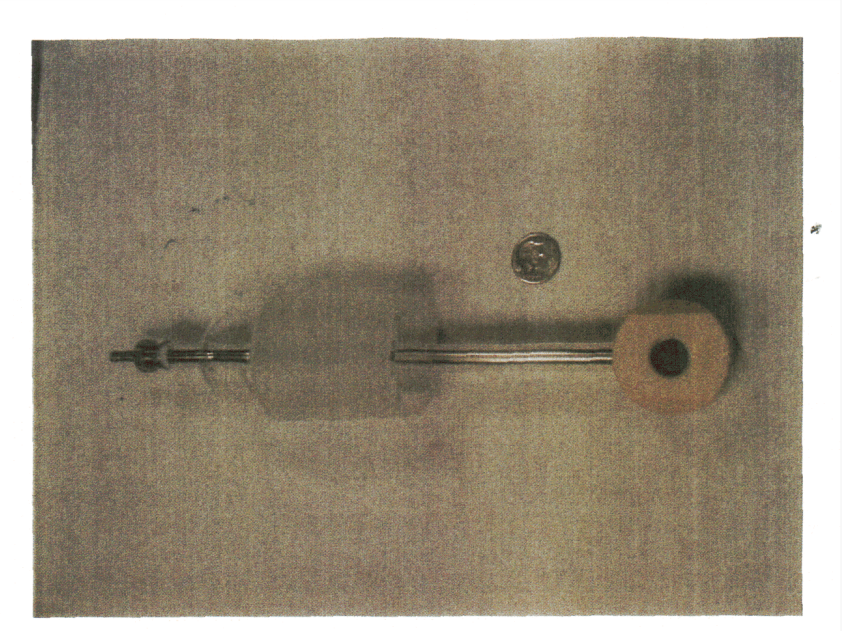

Figure 3: Assembly of disc specimens for electrochemical testing

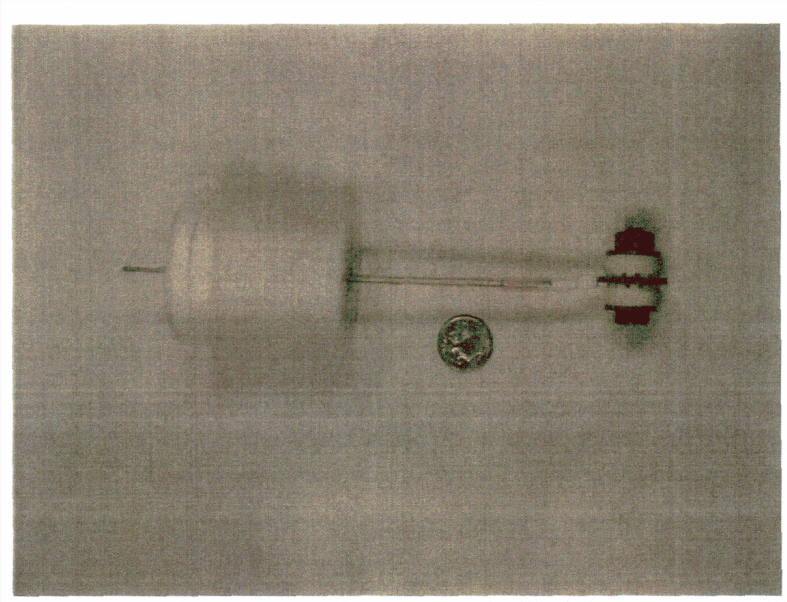

Figure 4: Assembly of MCA specimens for electrochemical testing.
Each specimen contains 24 creviced points where crevice corrosion may start.

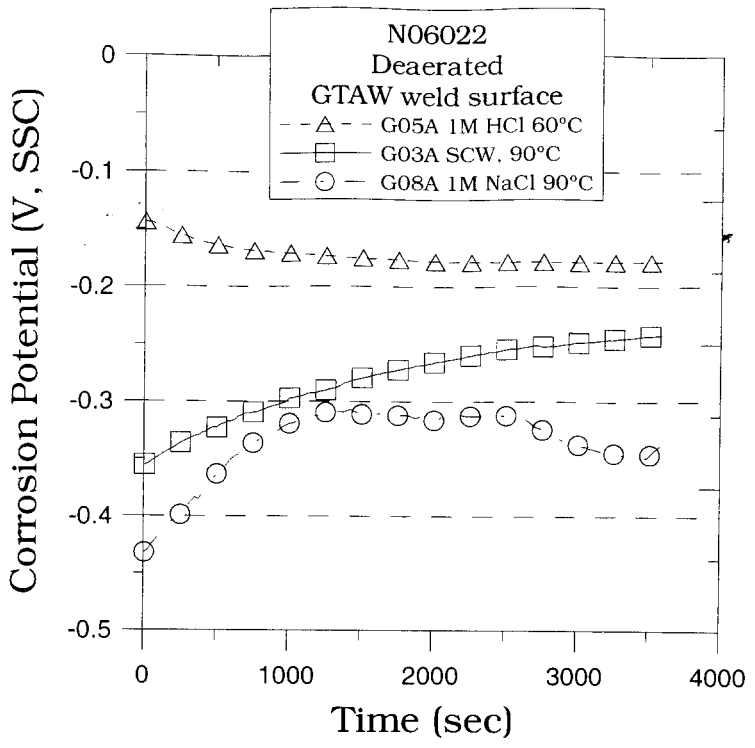

Figure 5: One hour corrosion potention (E_{corr}) versus time plot for GTAW specimens.

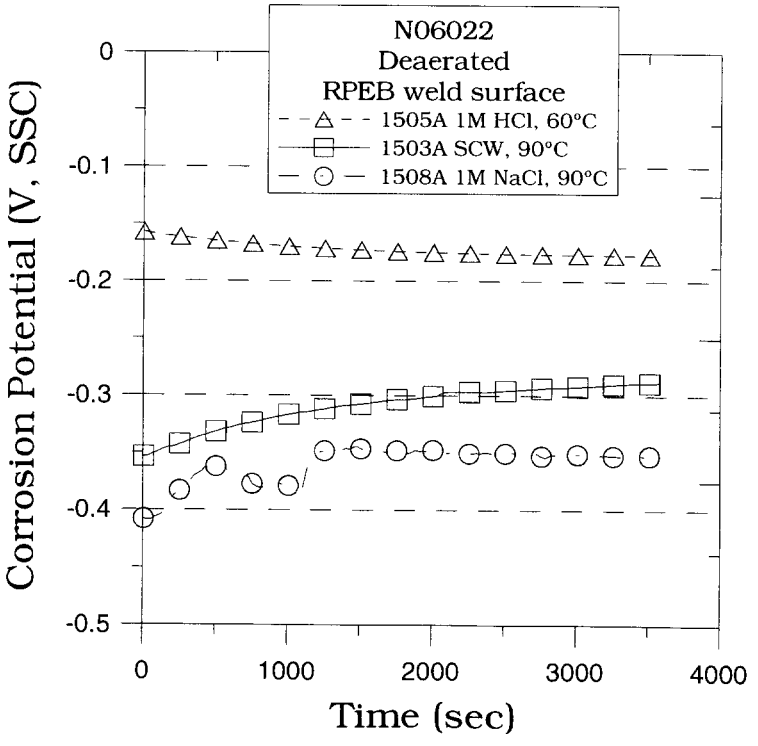

Figure 6: One hour corrosion potention (E_{corr}) versus time plot for RPEB specimens.

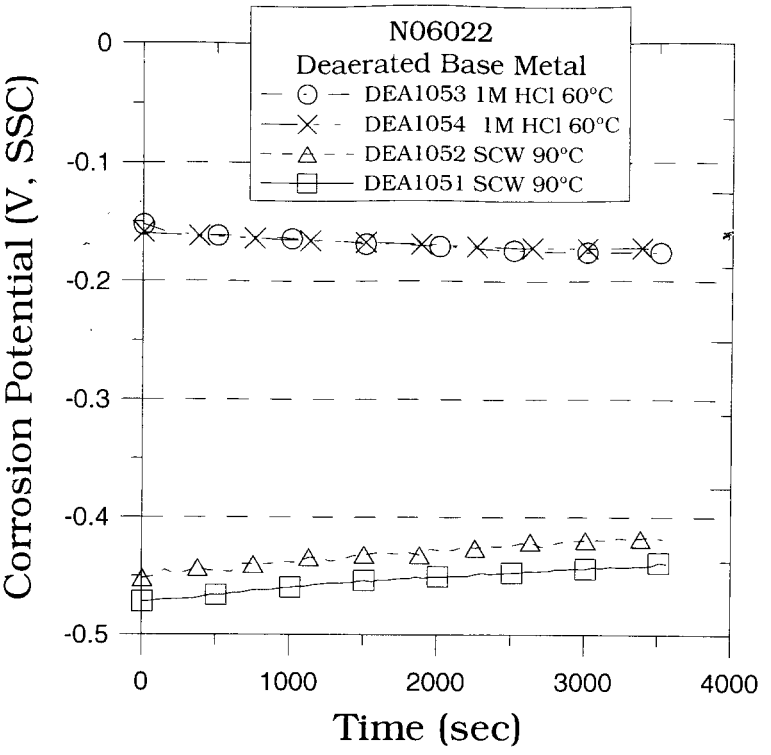

Figure 7: One hour corrosion potention (E_{corr}) versus time plot for base metal specimens.

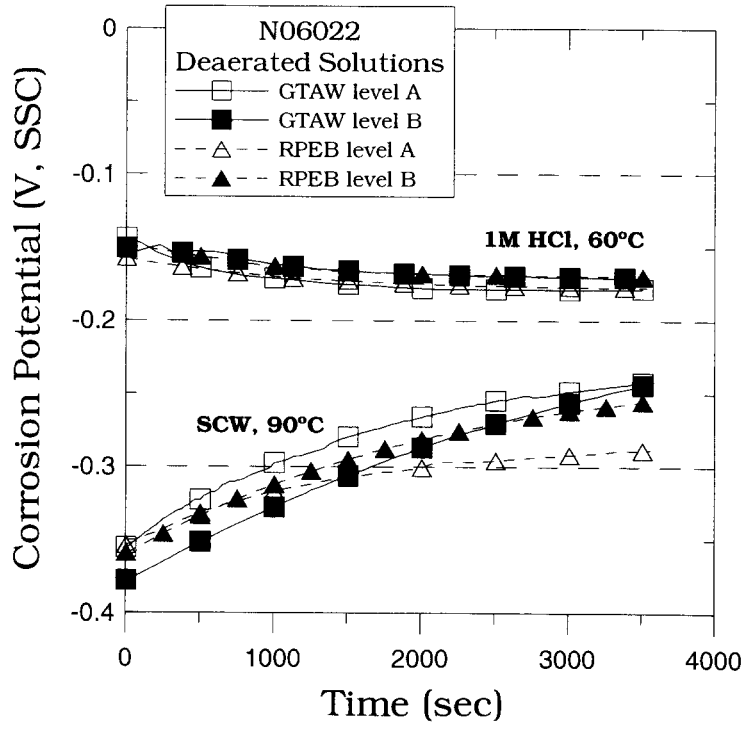

Figure 8: One hour corrosion potention (E_{corr}) versus time plot for weld specimens from different levels in the Alloy 22 plate.

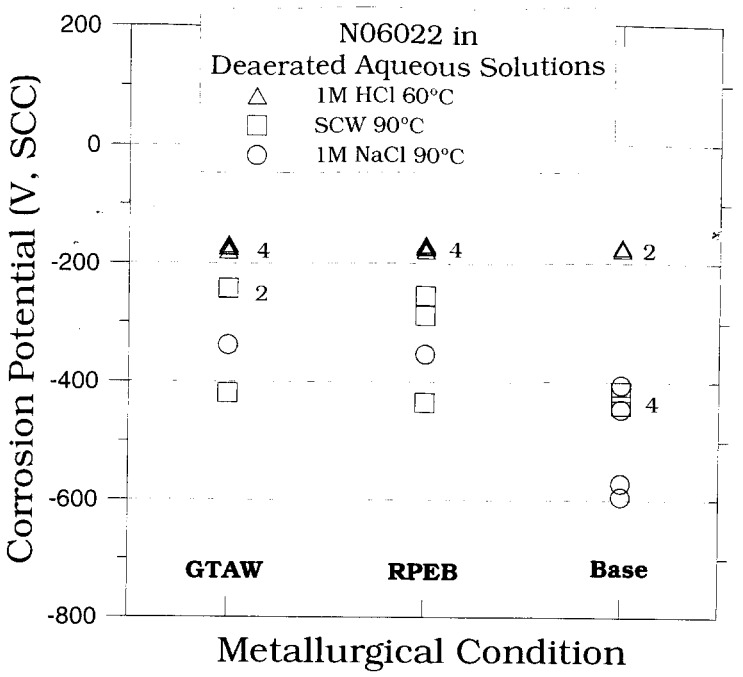

Figure 9: One hour corrosion potentials (E_{corr}) for welded and non-welded material. The values for base in 1 M NaCl correspond to 24 h immersion.

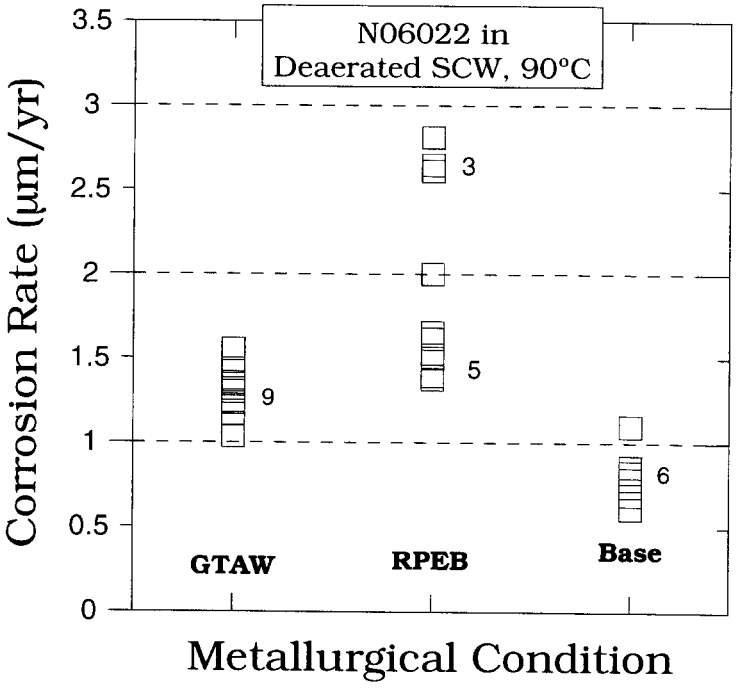

Figure 10: Corrosion rate for the three metallurgical states in 90°C SCW. Numbers indicate points in each cluster. Data from Table 2.

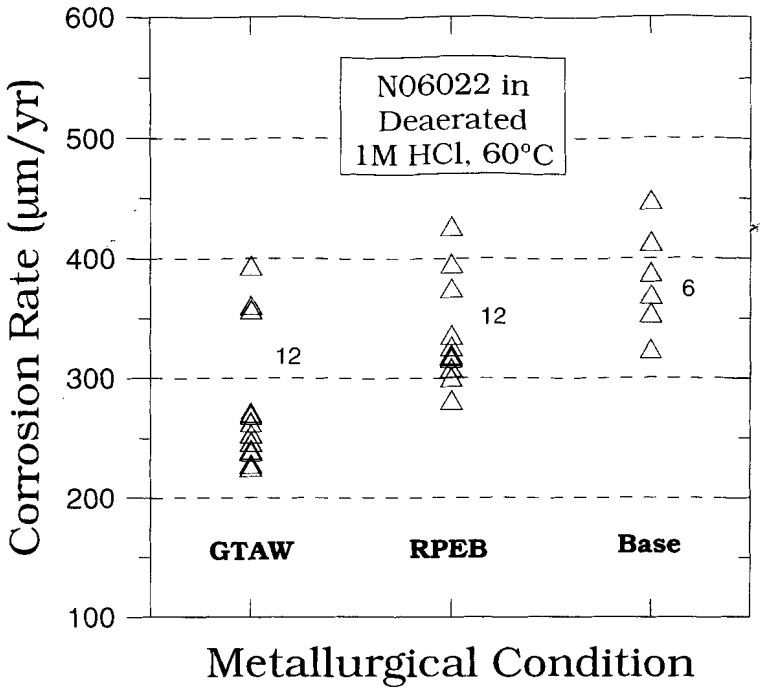

Figure 11: Corrosion rate for the three metallurgical states in 60°C 1M HCl. Numbers indicate points in each cluster. Data from Table 2.

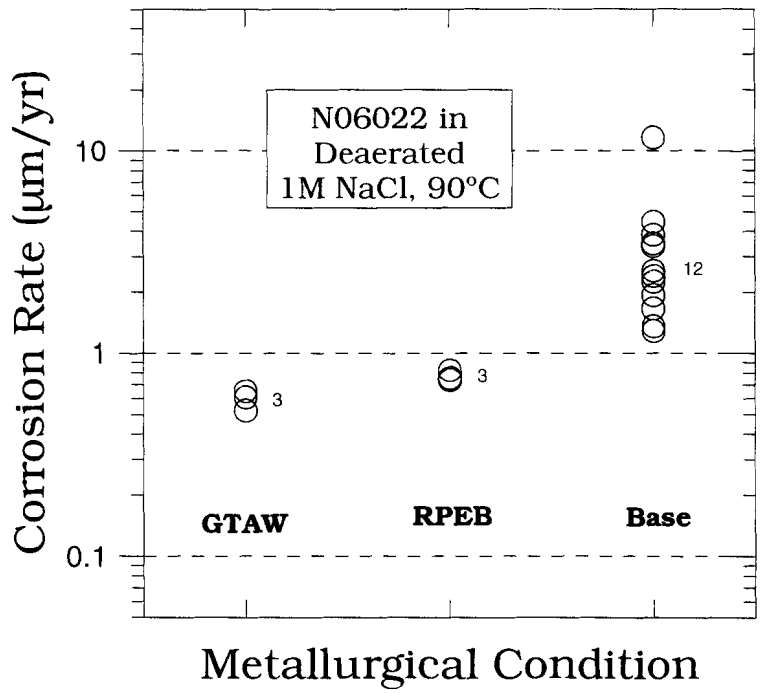

Figure 12: Corrosion rate for the three metallurgical states in 90°C 1M NaCl. Numbers indicate points in each cluster. Data from Table 2.

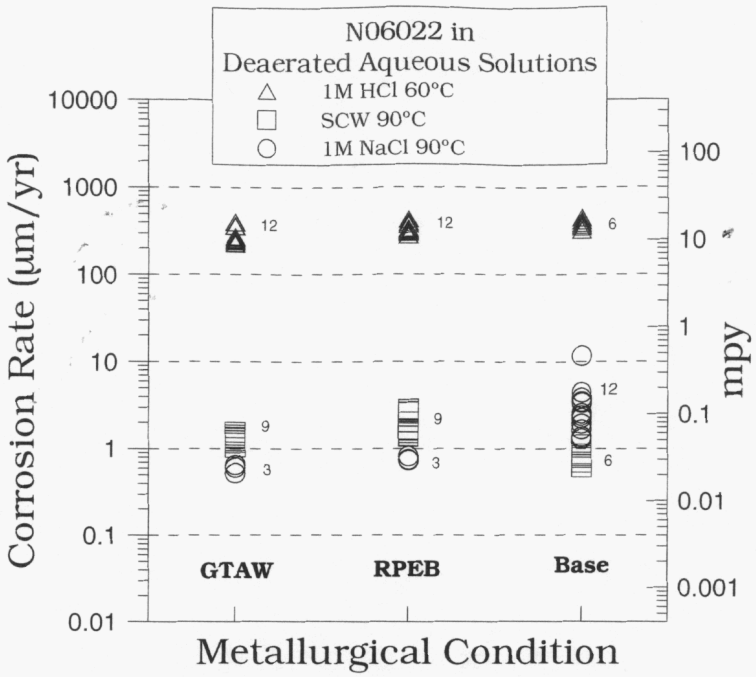

Figure 13: Corrosion rate versus metallurgical state for GTAW, RPEB weld, and base metal specimens in SCW, 1M HCl, and NaCl solutions. The small numerals next to the symbols indicate the number of individual points in each cluster.

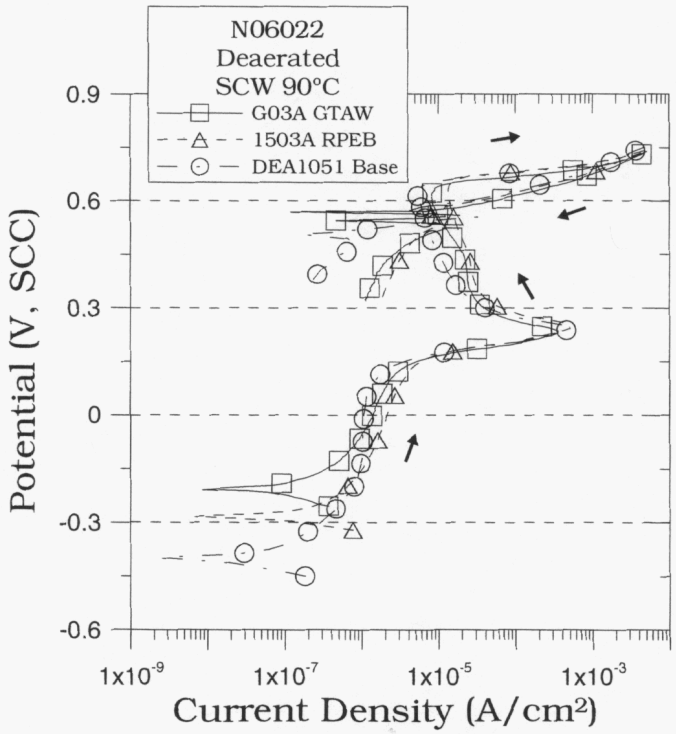

Figure 14: Cyclic polarization curves for the two Alloy 22 weld types and base metal in deaerated 90°C SCW. Arrows indicate the direction of curve trace as the test proceeds.

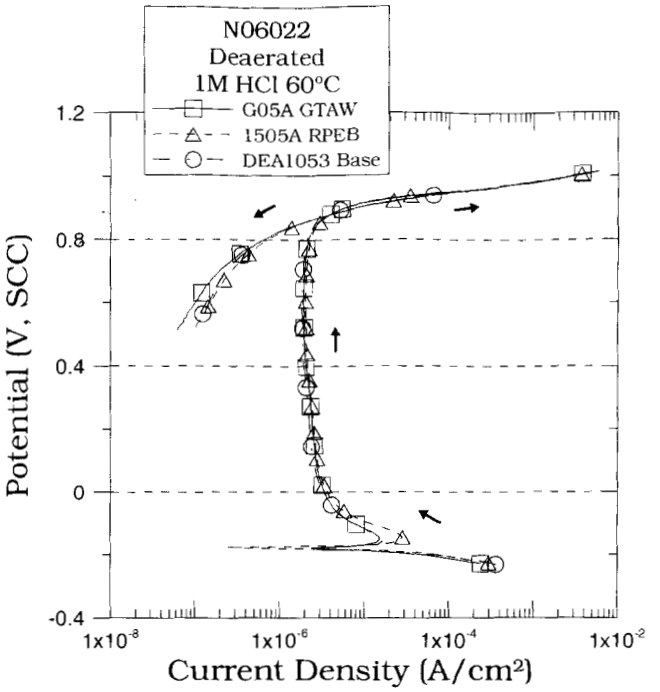

Figure 15: Cyclic polarization curves for the two Alloy 22 weld types and base metal in deaerated 60°C 1M HCl. Arrows indicate the direction of curve trace as the test proceeds.

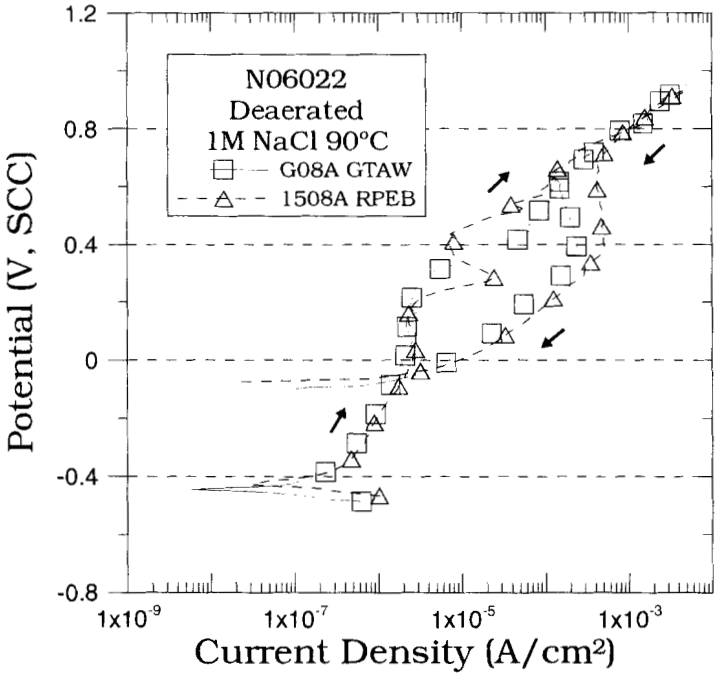

Figure 16: Cyclic polarization curves for the two Alloy 22 weld types and base metal in deaerated 90°C 1M NaCl. Arrows indicate the direction of curve trace as the test proceeds.

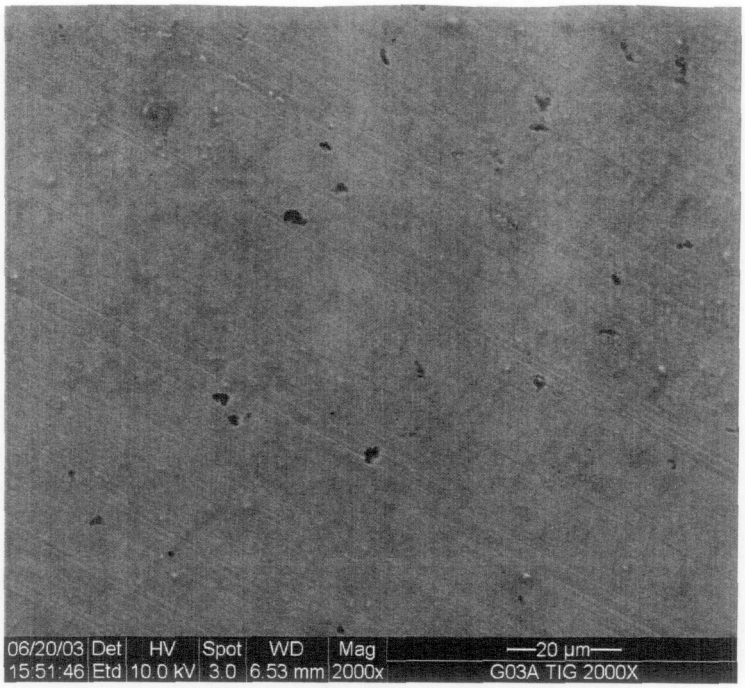

Figure 17: SEM image of specimen G03A GTAW after the cyclic polarization curve in SCW at 90°C

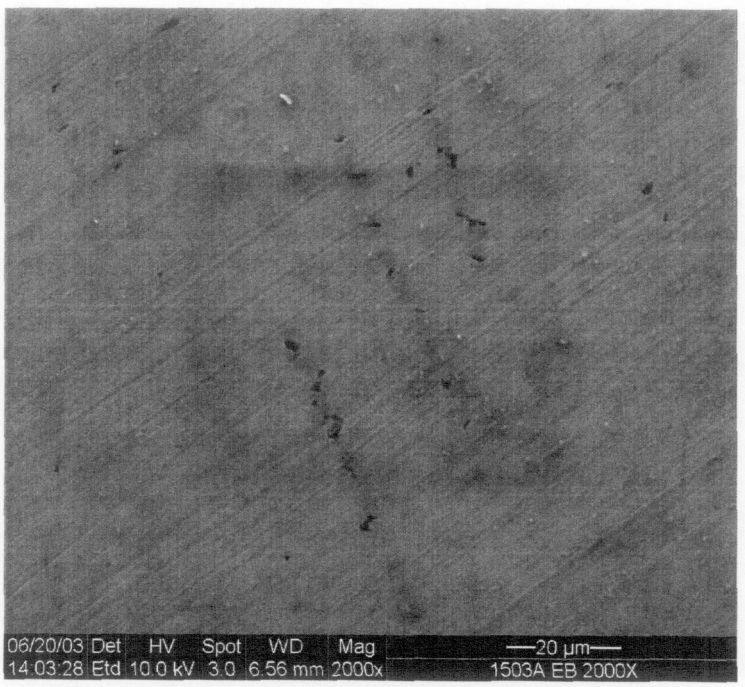

Figure 18: SEM image of specimen 1503A RPEB after the cyclic polarization curve in SCW at 90°C

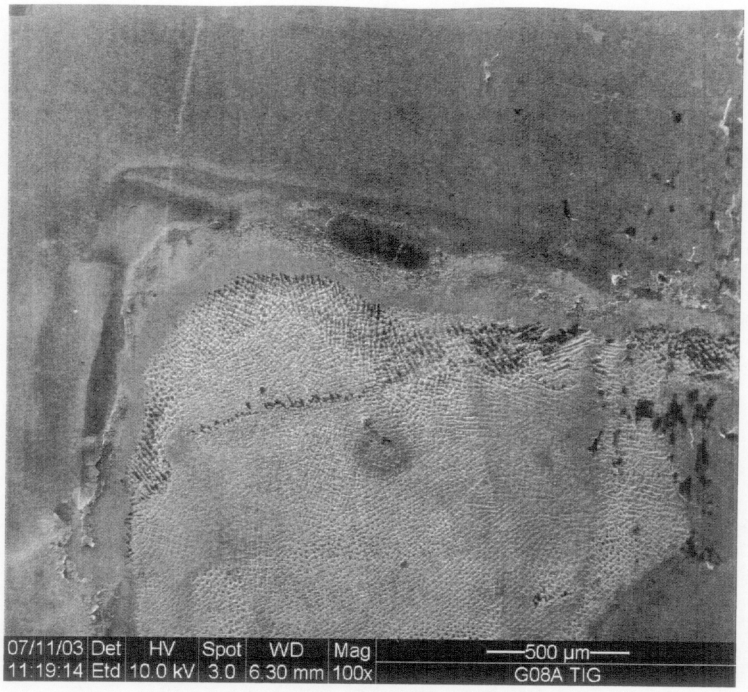

Figure 19: Localized corrosion in GTAW specimen G08A in 1 M NaCl at 90°C
100 X magnification

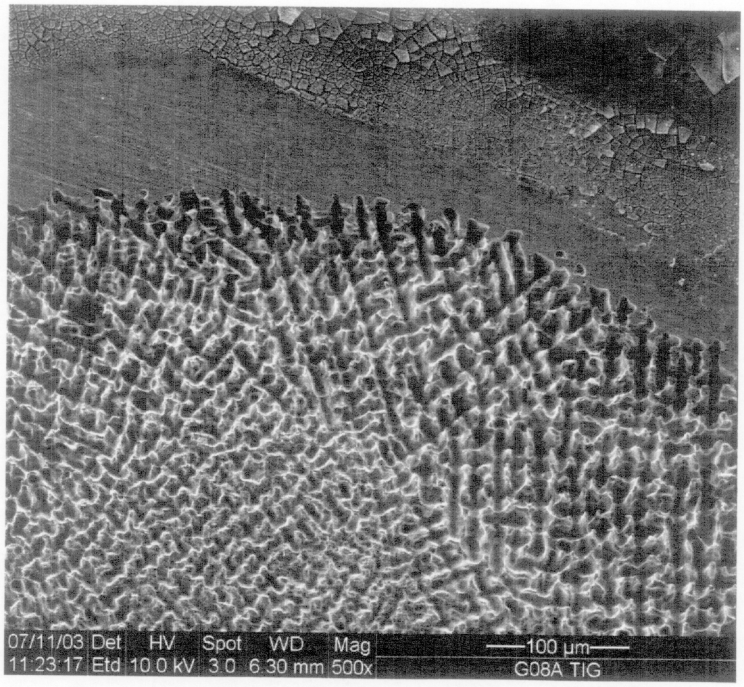

Figure 20: Localized corrosion in GTAW specimen G08A in 1 M NaCl at 90°C
500 X magnification

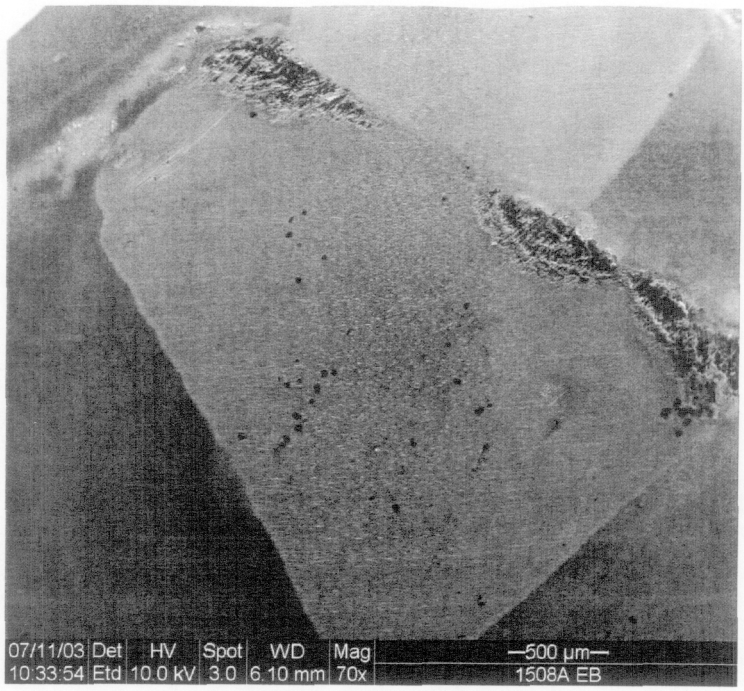

Figure 21: Localized corrosion in RPEB specimen 1508A in 1 M NaCl at 90°C
70 X magnification

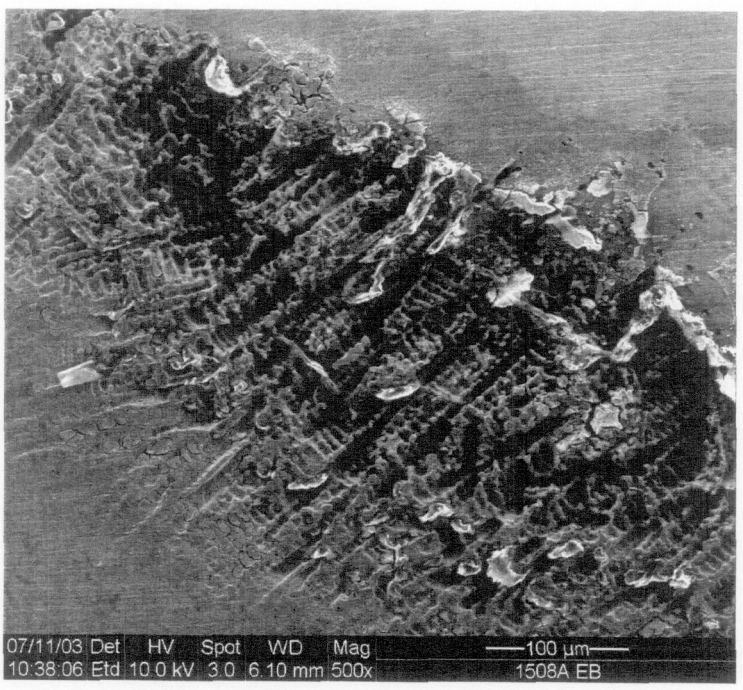

Figure 22: Localized corrosion in RPEB specimen 1508A in 1 M NaCl at 90°C
500 X magnification

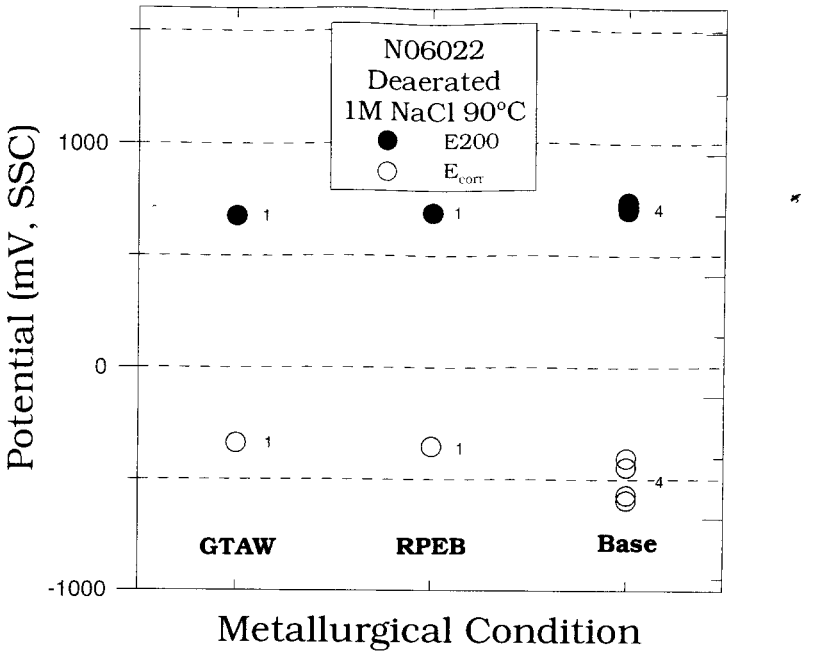

Figure 23: E200 and open circuit potentials (E_{corr}) for the two weld types and base metal disks in 90°C 1M NaCl. The numerals indicate the number of points in the symbol clusters.

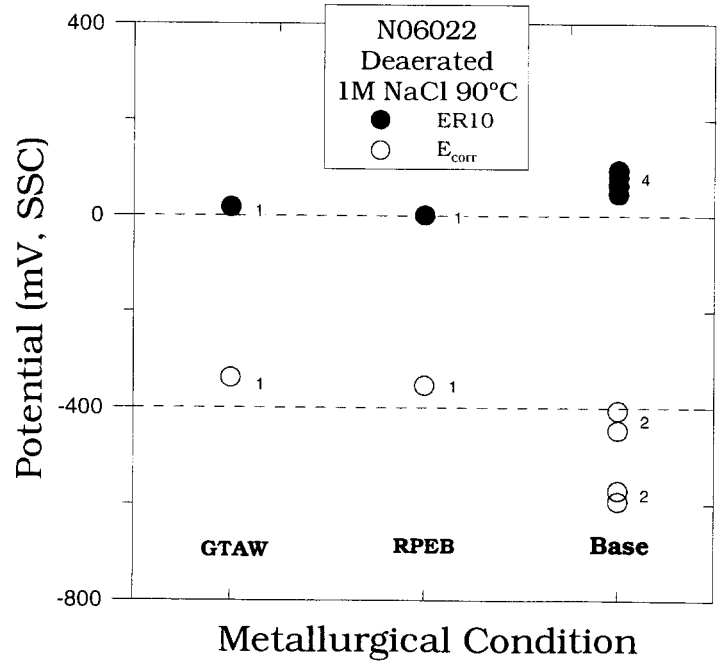

Figure 24: ER10 and open circuit potentials (E_{corr}) for the two weld types and base metal disks in 90°C 1M NaCl. The numerals indicate the number of points in the symbol clusters.

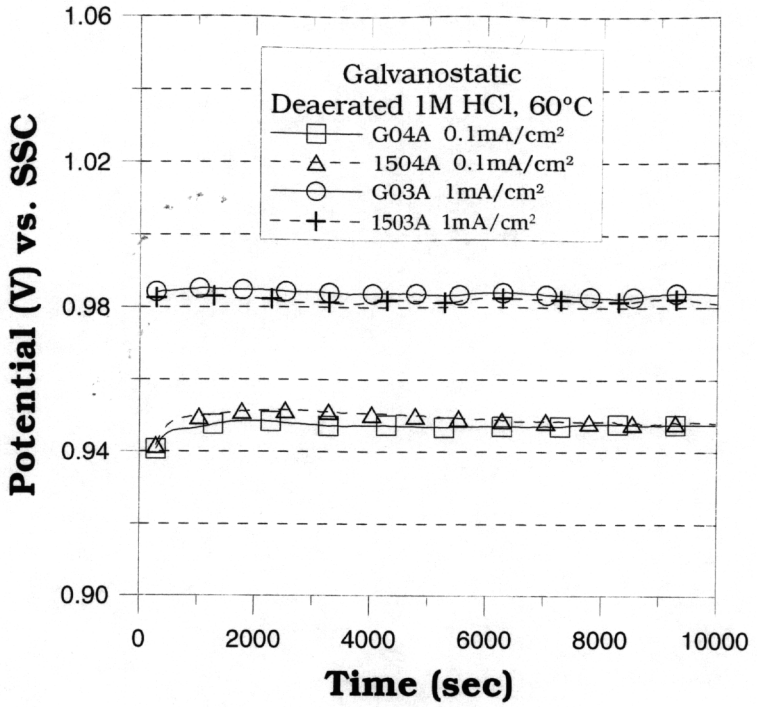

Figure 25. Galvanostatic test results for the GTAW and RPEB in 60°C 1M HCl. The first 10,000 seconds of the 3 hour test are plotted to show the similar behavior of the two welds during the galvanostatic testing.

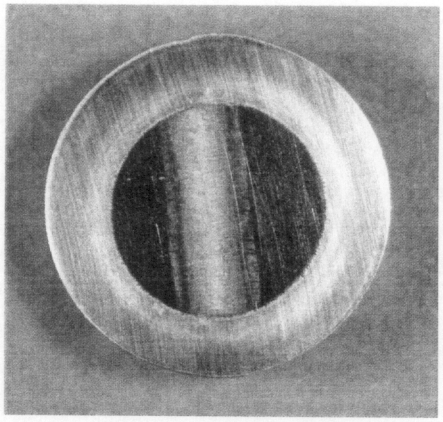

Figure 26: Specimen 1503A (RPEB) after galvanostatic test of 1 mA/cm² for 3 h in 1 M HCl at 60°C. Approximately X4.

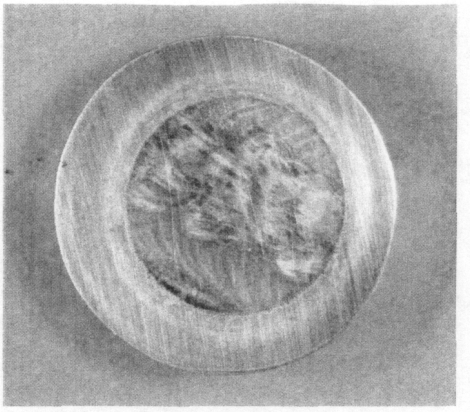

Figure 27: Specimen G03A (GTAW) after galvanostatic test of 1 mA/cm² for 3 h in 1 M HCl at 60°C. Approximately X 4.

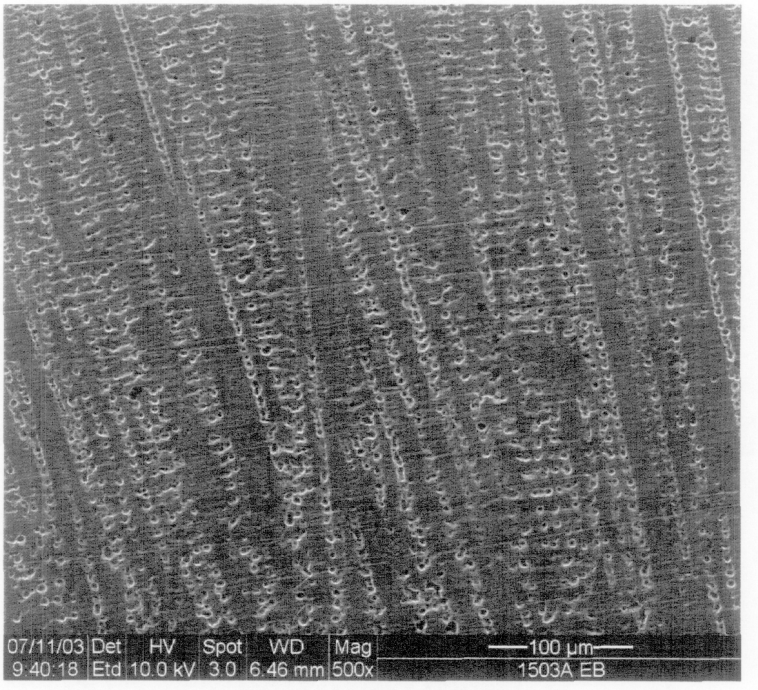

Figure 28: Corroded surface of RPEB specimen (1503A) after 1 mA/cm² galvanostatic testing in 1 M HCl at 60°C for 3 h.
500 X magnification

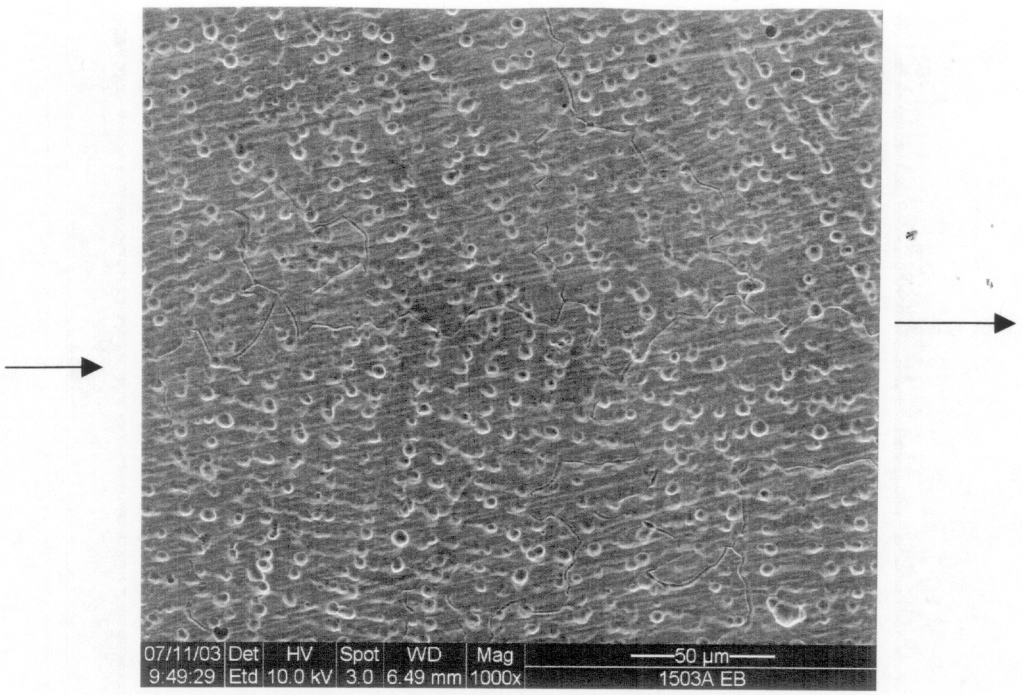

Figure 29: Corroded surface of RPEB specimen (1503A) after 1 mA/cm² galvanostatic testing in 1 M HCl at 60°C for 3 h. Fusion line.
1000 X magnification

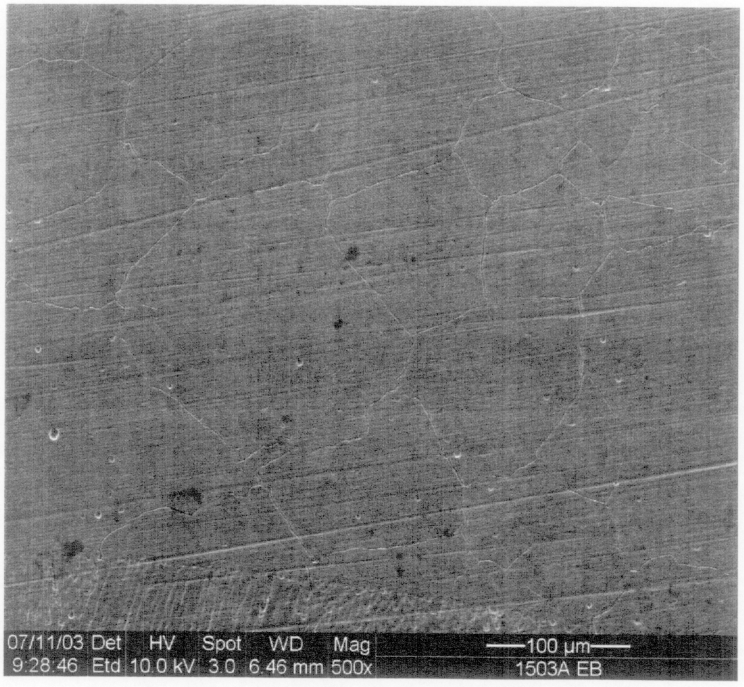

Figure 30: Grain boundary etching on the surface of the base metal of RPEB specimen (1503A) after 1 mA/cm² galvanostatic testing in 1 M HCl at 60°C for 3 h. The weld seam is shown towards the bottom of the picture. 500 X magnification

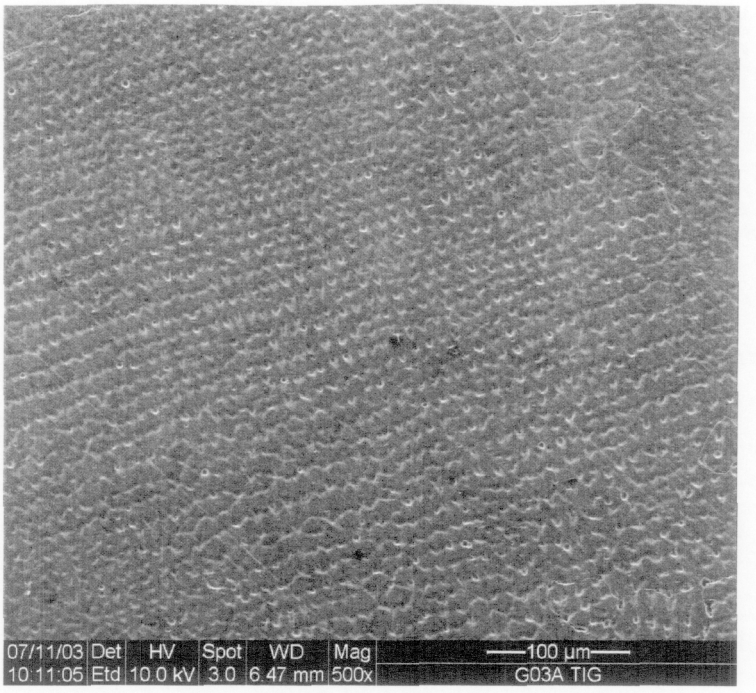

Figure 31: Corroded surface of GTAW specimen (G03A) after 1 mA/cm² galvanostatic testing in 1 M HCl at 60°C for 3 h.
500 X magnification

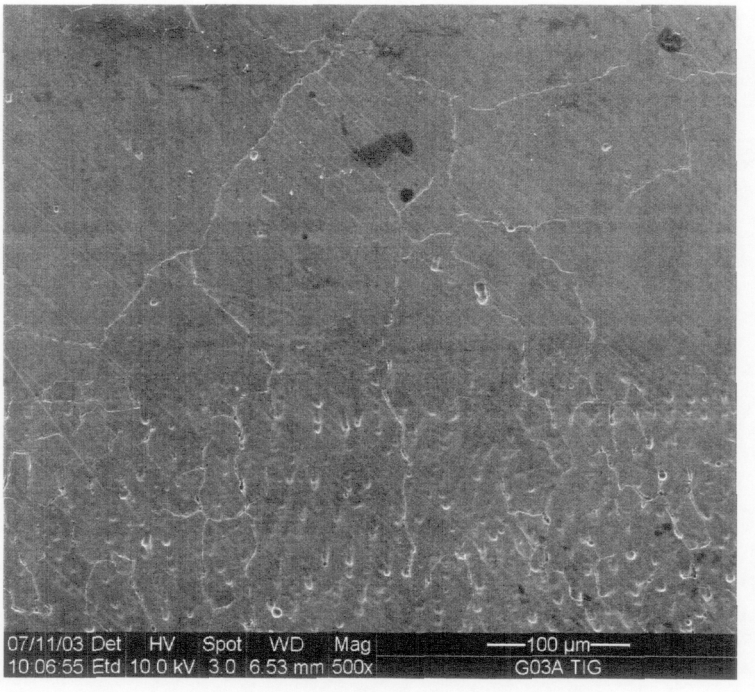

Figure 32: Grain boundary etching on the surface of the base metal of GTAW specimen (G03A) after 1 mA/cm² galvanostatic testing in 1 M HCl at 60°C for 3 h. The weld seam can be seen towards the bottom of the picture.
500 X magnification